J Mater Sci (2016) 51:10166–10177

Phase transformation, oxidation stability, and electrical conductivity of TiO_2-polysiloxane derived ceramics

Kathy Lu[1,*], Donald Erb[1], and Mengying Liu[1]

[1] *Department of Materials Science and Engineering, Virginia Polytechnic Institute and State University, Blacksburg, VA 24061, USA*

Received: 1 June 2016
Accepted: 20 July 2016
Published online: 27 July 2016

ABSTRACT

There have been increasing needs for high-thermal stability and high-electrical conductivity materials. In this study, we in situ synthesized silicon oxycarbide (SiOC)–TiC_xO_y composites based on the pyrolysis of polysiloxane and carbothermal reaction between TiO_2 nanoparticles and free carbon in SiOC. The TiO_2 to TiC_xO_y conversion is dependent on the pyrolysis temperature. Higher pyrolysis temperature leads to more TiC formation but lower thermal stability. With more homogeneous distribution of TiO_2, the thermal stability of the SiOC–TiC_xO_y composite increases. This family of SiOC composite also demonstrates high electrical conductivity. The highest electrical conductivity is 5.03 S cm^{-1} at 400 °C measurement temperature, the highest for air atmosphere condition. The key issue for tuning the SiOC–TiC_xO_y system for both thermal stability and electrical conductivity is to avoid the destabilization of the SiOC system.

Introduction

Compared to conventional ceramics prepared by sintering corresponding powders, polymer-derived ceramics (PDCs) exhibit many unusual properties that are tailorable from polymer precursors [1]. The synthesis process starts with liquid polymer crosslinking, and the composite can be made into almost any shape (bulk, coating, etc.) and size based on the application needs. Also, polymer-derived ceramics have excellent thermophysical properties. For example, silicon oxycarbides (SiOCs) can be used as high-temperature-resistant structural materials (automotive, aerospace, etc.), hard materials, chemical engineering components (catalyst support, food and biotechnology, etc.), or functional materials as in micro/nanoelectronics [2, 3]. Inert or active fillers can be easily introduced into the polymer during crosslinking to change their shaping abilities, thermomechanical behaviors, and other functional properties. Example fillers such as ZrO_2, HfO_2, SiC, B_4C, Si_3N_4, BN, Ti, Cr, V, Mo, Si, and B have been added into the PDCs to improve their near-net-shape conversion ability, thermal stability, and mechanical properties [1, 4–7]. The tunable thermophysical properties together with the microfabrication capability and excellent high temperature thermal and

Kathy Lu—Member of American Ceramic Society.

Address correspondence to E-mail: klu@vt.edu

DOI 10.1007/s10853-016-0244-6

mechanical properties make the filler modified SiOC excellent candidate materials for high-temperature sensors, electrode materials, coatings, etc.

With the addition of fillers, the high temperature stability of carbon-rich SiOCs can be altered. The intertwining relationships between the composition, microstructure, and thermal stability present not only scientific intrigues but also application challenges [8–10]. Recently, electrical properties of PDCs have become increasingly important, stimulated by their potential applications in many important fields, such as harsh environmental microelectromechanical systems/microsensors and electrode materials for energy storage devices [11–15]. Some magnetic materials, for example, Fe, Co, and Ni particles, are incorporated into the polymer to offer new capabilities for automotive, electronic, space, and instrumentation applications [16]. However, the microstructure and the homogeneity of the as-synthesized PDC composites can be influenced by the particle size and the reactivity of the metal powders. Due to their high sensitivity to oxygen and moisture, it is difficult to use nanosized metal powders as fillers in the composites for electrical conductivity gain. The corresponding chlorides ($FeCl_2$, $CoCl_2$) and organics ($Fe(CO)_5$, $Fe(AcAc)_3$) are usually used as fillers to modify the PDCs [17–22]. The drawbacks are that these additives are often expensive and the filler volume percent is limited. $MoSi_2$ powders, as a non-metallic high temperature conductor, have also been added into SiOCs to improve their electrical conductivity [23, 24]. The problem is that when the carbon content or pyrolysis temperature is high, $MoSi_2$ reacts with free carbon in SiOCs to form carbide because free carbon has high activity in an inert atmosphere during pyrolysis [1].

With the above considerations, there is one candidate material that shows the great potential to deliver both high thermal stability and electrical conductivity. This material is TiO_2. TiO_2 nanoparticles are widely available and can be added into the polymer system during crosslinking. During pyrolysis, TiO_2 is known to react with carbon at high temperatures to form conducting TiC through carbothermal reactions, which has excellent high temperature stability. Also, TiC has excellent oxidation resistance and electrical conductivity of 5000–7500 S cm^{-1} at room temperature [25–27]. Submicron scale TiC–C hybrid nanofibers have been synthesized by carbothermal reduction of TiO_2 with carbon at high temperatures [28]. The mixture of TiO_2 and carbon resin was reacted at 1500 °C under flowing Argon atmosphere to form TiC [27]. Uniformly mixed TiO_2 and graphite powders were heated up to 1600 °C in Argon, forming several intermediate oxides before ultimately forming a solid solution of TiO_xC_y [29]. TiO_2 layer deposition on carbon by a sol–gel process and then a heat treatment above 1400 °C also led to the formation of TiC [30]. However, TiO_2 introduction into the SiOC system for TiC formation has not been closely examined, and the actual electrical conductivity for the SiOC–TiC composite is unknown. For the polyhydromethylsiloxane (PHMS) plus divinylbenzene (DVB) system, the C-rich nature during the pyrolysis should provide an excellent opportunity for TiC formation and thus impact the corresponding material's electrical conductivity.

In this study, we in situ synthesized SiOC–TiC_xO_y composites utilizing the reaction between TiO_2 nanoparticles and the free carbon in SiOC during pyrolysis. The phase transformation behavior and the thermal stability of the samples pyrolyzed under different conditions are analyzed. The resulting electrical conductivity is systematically studied. Further strategies of tuning the SiOC–TiC_xO_y system for both thermal stability and electrical conductivity are presented.

Experimental procedure

In this work, PHMS (Gelest Inc., Morrisville, PA) was chosen as the precursor, DVB (Sigma-Aldrich, St. Louis, MO) was used as the crosslinking agent, and 2.1–2.4 % platinum-divinyltetramethyldisiloxane complex in xylene (Pt catalyst, Gelest Inc., Morrisville, PA) was used as the catalyst. Toluene (Fisher Scientific, Pittsburgh, PA) was used as the solvent, and TiO_2 nanopowder (anatase, average particle size <25 nm, Sigma-Aldrich, St. Louis, MO) was used as the filler material.

First, TiO_2 powder and toluene were mixed with a ratio of 0.03 g TiO_2 per mL of toluene and milled in a high energy mill (SPEX 8000 M Mixer/Mill, SPEX SamplePrep, Metuchen, NJ) for 10 min. Next, PHMS and DVB (60 wt% relative to PHMS) were added to the milled mixtures to create samples with 10, 20, and 30 wt% TiO_2 (relative to PHMS); additionally, a 0 wt% TiO_2 sample was created as the baseline. The mixtures were then milled further for 25 min. Then

the diluted Pt catalyst (5 ppm relative to PHMS) was introduced into the mixtures. The mixtures were milled for two additional minutes and then placed in aluminum molds and vacuumed at 1500 mTorr to remove any air bubbles. Next, they were placed in an oven to cure at 50 °C for 12 h, 80 °C for 10 h, and at 120 °C for 6 h; the cured materials were hard and tan colored.

In order to improve the dispersion of TiO_2 nanoparticles within the solution and then the resulting composite, surface modified TiO_2 particles were created as follows: First, surfactant sodium dodecyl sulfate (SDS, Fisher Scientific, Pittsburgh, PA) was mixed with deionized water and TiO_2 at a concentration below the critical micelle concentration of SDS. In this case, the concentration of SDS in the deionized water was approximately 0.0014 g/mL. Next, the mixture was milled for 30 min. After milling, the TiO_2 particles were covered by the brush-like SDS and naturally separated from the water solution. The separated particles were then removed from the surface of the solution, rinsed with ethanol, and then vacuumed until the ethanol, and any remaining water had evaporated. After functionalization, the powder contained roughly 6.5 wt% SDS. A sample containing 30 wt% of the surface modified TiO_2 particles was then prepared following the same procedures as listed above.

To prepare the samples for pyrolysis, the cured materials were first cut and polished to roughly 10 mm × 10 mm × 1.5 mm size. Next, the samples were placed into a zirconia boat, covered on both sides with graphite mats in order to prevent oxidation, and put into a tube furnace (1730–12 Horizontal Tube Furnace, CM Furnaces Inc., Bloomfield, NJ). With an Ar flow rate of about 16 std cm^3/s, the samples were heated up to 800 °C with a rate of 1 °C/min, held at this temperature for 2 h, then heated up to 1200, 1300 or 1400 °C at a rate of 1 °C/min, and held for 2 h for pyrolysis. The shrinkage, ceramic yield, and density of the samples during the pyrolysis were tracked.

Phase compositions of the pyrolyzed samples were analyzed in an X'Pert PRO diffractometer (PANalytical B.V., EA Almelo, The Netherlands) with Cu Kα radiation. The JCPDS reference cards used to identify the crystalline phases were 00-039-1425 for SiO_2, 01-075-1621 for C, 00-029-1129 for SiC, 01-086,0147 for rutile TiO_2, 01-071-1054 for Ti_2O_3, 01-082-1137 for Ti_3O_5, 01-075-1621 for Ti_4O_7, 01-086-2352 for TiO, and 01-086-2352 for TiC. Densities were measured based on the dimensions and mass of regularly shaped samples. The thermal stability of the SiOC samples after pyrolysis was investigated by thermogravimetric analysis (TGA) and differential scanning calorimetry (DSC) using a STA 449C Jupiter® analyzer (Netzsch-Gerätebau GmbH, Selb, Germany) with a temperature range of room temperature to 1000 °C, a heating rate of 5 °C/min, and an air flux of 40 ml/min. The electrical conductivity of the samples was measured in air from room temperature up to 500 °C in a four-point probe configuration using a potentiostat (VersaSTAT 3, Princeton Applied Research, Oak Ridge, TN). A field emission SEM (LEO 1550, Carl Zeiss MicroImaging, Inc . Thornwood, NY) and an energy dispersive X-ray spectroscopy (QUANTAX 400, Bruker AXS, Madison, WI) attached to an environmental SEM (Quanta 600 FEG, FEI, Hillsboro, OR) were used to characterize the microstructures and elemental distributions of the pyrolyzed samples.

To examine the sizes of the SiO_2 nanoclusters with and without the TiO_2 additive, 0 wt% TiO_2 and 30 wt% TiO_2 SiOC samples pyrolyzed at 1400 °C were etched in a hydrofluoric acid solution (20 wt% HF in water). The solution was magnetically stirred at room temperature until there was no significant mass loss from the samples; the samples were then rinsed with water and dried at 120 °C. Nitrogen adsorption was conducted on the etched samples using a Quantachrome Autosorb-1C (Quantachrome Instruments, Boynton Beach, FL), and the pore size distributions were derived by applying the Non-Local Density Functional Theory (NLDFT) to the adsorption branch of the data.

Results and discussion

Thermophysical properties

All the samples have good shape and integrity after pyrolysis. Compared to pure SiOC systems [31], the TiO_2 filler reduces or eliminates defects by lowering the shrinkage and thermal stress during the pyrolysis. Table 1 shows the volume shrinkage, ceramic yield, and density values for the samples after the pyrolysis.

The volume shrinkage values for all of the samples are in the range of 45–52 %. At the same pyrolysis temperature, as the TiO_2 content increases, the volume shrinkage steadily decreases. This is because TiO_2 is a filler material and does not experience as much

Table 1 Volume shrinkage, ceramic yield, and density of pyrolyzed SiOC–TiC_xO_y samples

TiO_2 Content (wt %)	Volumetric shrinkage (%)			Ceramic yield (%)			Density (g/cm^3)		
	1200 °C	1300 °C	1400 °C	1200 °C	1300 °C	1400 °C	1200 °C	1300 °C	1400 °C
0	51.80 ± 2.15	50.58 ± 0.09	49.57 ± 2.33	83.36 ± 0.11	83.47 ± 0.14	83.23 ± 0.35	1.86 ± 0.14	1.71 ± 0.01	1.83 ± 0.10
10	51.19 ± 0.54	51.15 ± 1.92	49.14 ± 0.75	84.33 ± 1.78	82.99 ± 0.46	82.35 ± 0.72	1.91 ± 0.11	1.82 ± 0.04	1.87 ± 0.01
20	49.63 ± 1.73	49.05 ± 0.57	46.04 ± 0.21	84.47 ± 1.96	82.71 ± 0.28	82.40 ± 0.35	1.98 ± 0.08	1.77 ± 0.01	1.76 ± 0.06
30	48.65 ± 4.48	45.71 ± 0.14	45.89 ± 2.55	84.11 ± 2.95	82.88 ± 0.22	82.74 ± 0.77	2.01 ± 0.18	1.70 ± 0.01	1.92 ± 0.12

shrinkage as polymer decomposition during the pyrolysis even with the consideration of carbothermal reactions between TiO_2 and carbon. As a result, higher TiO_2 content leads to less shrinkage. However, some of the volume shrinkage values show large variations and overlapped values when the standard deviation is considered. For the same TiO_2 concentration, the volume shrinkage generally decreases as the pyrolysis temperature increases. Again, some of the volume shrinkage values show large variations and should not be regarded as a general trend. Overall, these results mean fairly large volume shrinkage.

The ceramic yield values for all of the samples range from 82–84.5 %. At the same pyrolysis temperature, an increase in the TiO_2 content shows no general effect on the ceramic yield. This means that the ceramic yield is determined by the polymer decomposition and TiO_2 to TiC conversion, likely to some similar extent. For the same TiO_2 concentration, the ceramic yield generally slightly decreases as pyrolysis temperature increases. This is understandable as PHMS and DBV generate more free carbon with pyrolysis temperature increase and thus potentially more weight loss through evaporative species. TiO_2 to TiC conversion can also contribute to the effect.

The densities for all of the samples are in the range of 1.70–2.01 g/cm^3. At 1200 °C pyrolysis temperature, as the TiO_2 content increases, the density increases. This is likely because of the more stable nature of TiO_2; more TiO_2 results in less mass loss from polymer decomposition. At 1300 and 1400 °C pyrolysis temperatures, however, there is no consistent density trend. We believe that this is due to the simultaneous processes of SiOC matrix weight loss and TiC formation. The density change is not significant considering the standard deviation of the measurements.

Summarizing the results in Table 1, it can be stated that the physical characteristics (shrinkage, ceramic yield, and density) of the resulting SiOC–TiC_xO_y samples remain relatively stable and experience only small changes in the wide temperature range of 1200–1400 °C. Even though the general understanding is that higher pyrolysis temperature should lead to larger shrinkage and lower ceramic yield, the reactive nature of the TiO_2 additive counters this effect.

Phase transformation

In Fig. 1, the phase transformation of the PHMS + DVB matrix with different TiO_2 content is

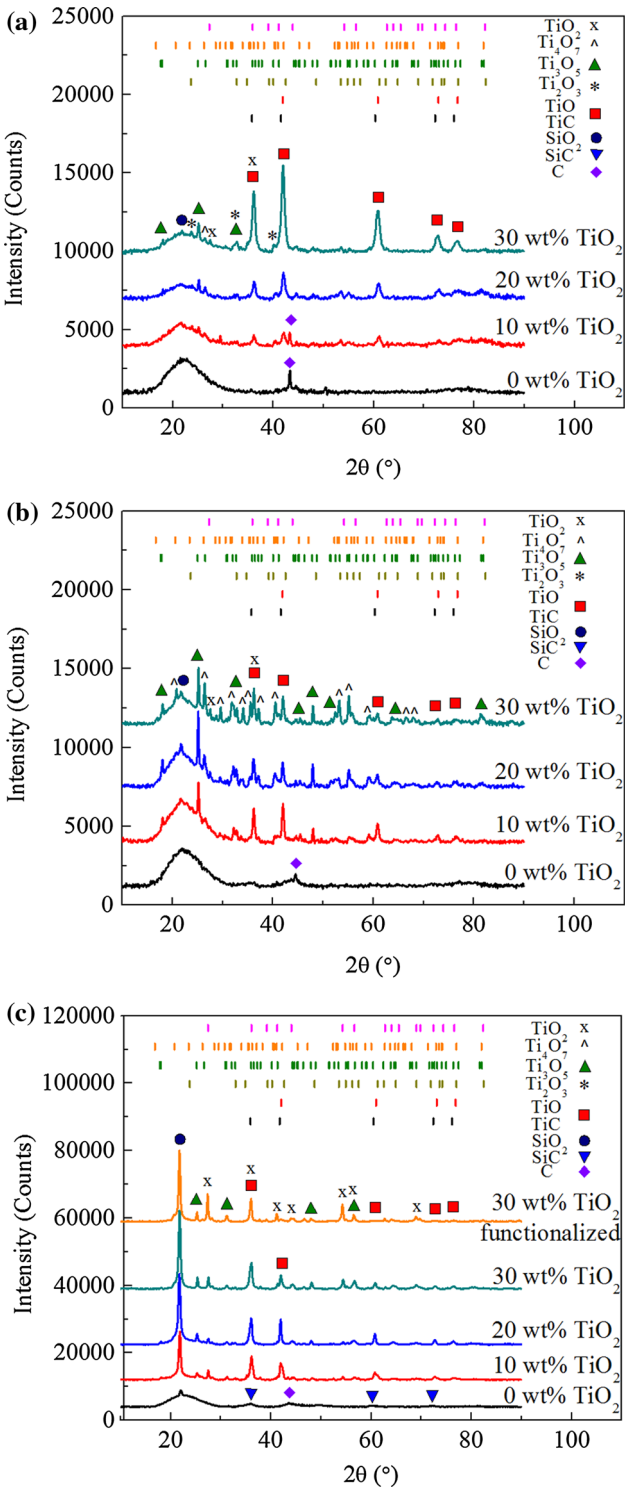

Figure 1 XRD patterns of PHMS + DVB matrix with different amount of TiO_2 additive after pyrolysis at **a** 1200 °C, **b** 1300 °C, and **c** 1400 °C for 2 h in flowing argon.

shown for different pyrolysis temperatures. At 1200 °C, with 0 wt% TiO_2, the 22.9° hump along with the weak 25° peak indicates that the SiO_2 formed is largely amorphous. The 43° peak corresponds to the (101) or (100) planes of graphene [32, 33]. This observation is consistent with typical SiOC systems. The high carbon content contributes to the hindered crystallization of SiO_2. With the TiO_2 content increase to 10 wt%, some minor peaks appear at 36°, 42°, and 61°, consistent with the formation of a small amount of cubic TiC_xO_y (mixture/solid solution of TiC and TiO). With the TiO_2 content increase to 20 and 30 wt%, these three peaks become stronger, an indication of more TiC_xO_y solid solution formation. In addition, Ti_3O_5 peaks begin to show at 18°, 25°, and 32.5°, as well as smaller peaks corresponding to Ti_4O_7 and Ti_2O_3 [26, 29]. At these higher TiO_2 content conditions, TiC_xO_y formation also leads to more SiO_2 formation, represented by the peak at 22.9°. This is consistent with the notion that the inhibiting effect from excessive carbon for SiO_2 phase transformation is decreased. Based on this observation, it can be stated that TiO_2 addition leads to less excessive carbon and more SiO_2, resulting in a mixture of amorphous SiO_2 and crystalline SiO_2. At the same time, TiC_xO_y forms, and its content increases with the initial TiO_2 content, supported by the increasing presence of the peaks at 36°, 42°, and 61°.

With the pyrolysis temperature increase to 1300 °C (Fig. 1b), the SiOC system with 0 wt% TiO_2 shows no obvious change compared to that of the 1200 °C pyrolysis condition. With the TiO_2 presence, however, the SiO_2 crystallizes further, demonstrated by the 22° hump change to a sharp peak. From 20° to 62°, a series of small peaks are present originating from a series of intermediate oxides due to TiO_2 reduction by C, such as Ti_3O_5 and Ti_4O_7, as well as TiC. Some rutile TiO_2 may also exist. Overall, higher TiO_2 content leads to more SiO_2, Ti_xO_y, and TiC_xO_y formation.

When the pyrolysis temperature is increased to 1400 °C (Fig. 1c), the strong 21.8° peak indicates the formation of tetragonal SiO_2. The peaks at 36°, 42°, and 61° indicate the TiC_xO_y presence. Comparing the TiC_xO_y peaks around 36° at 1200 and 1400 °C, a shift from 36.1° to 36° can be observed with the increase of the pyrolysis temperature. This indicates a higher carbon concentration in the TiC_xO_y solution (or formation of more TiC) because the peak of cubic TiC is centered at 36.0°, while the peak of cubic TiO is centered at 36.2°. Other tiny peaks are likely from residual titanium oxides, Ti_3O_5, and rutile TiO_2. With increasing TiO_2 content, these residual peaks increase, indicating the incomplete reaction and

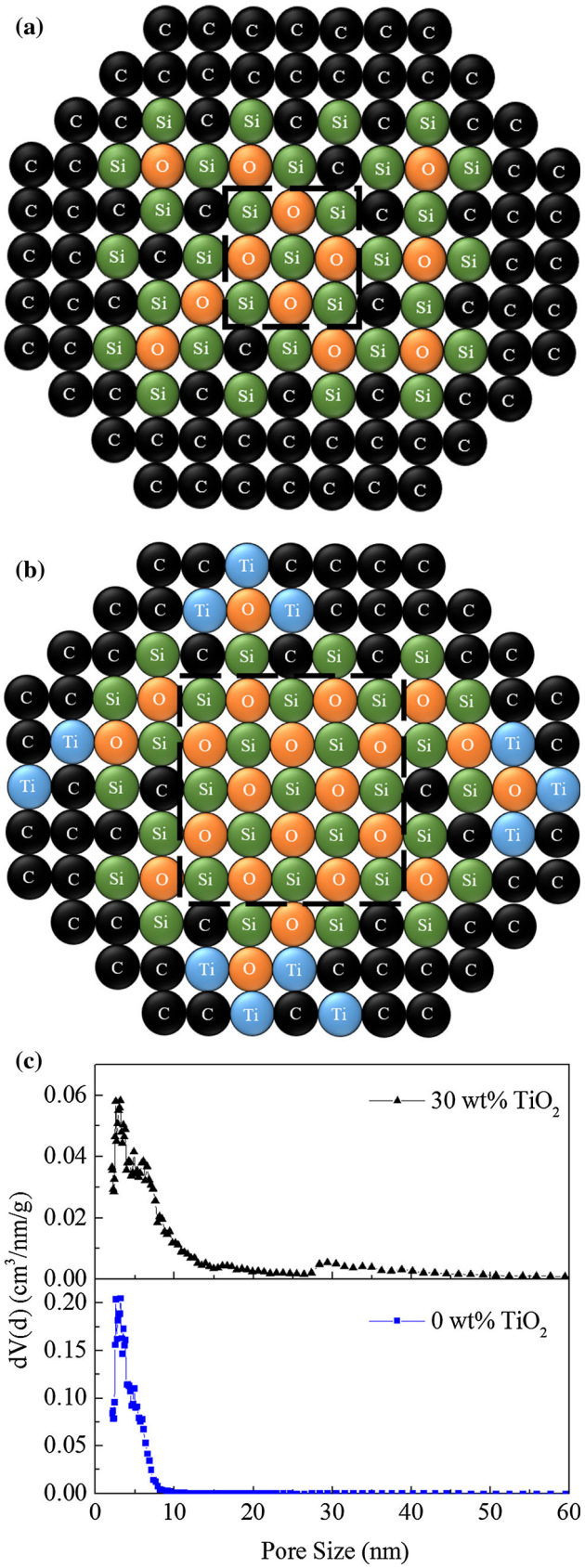

◀**Figure 2** Illustrations of coexisting species without TiO_2 additive (**a**) and with TiO_2 additive (**b**); **c** pore size distributions for the samples pyrolyzed at 1400 °C with and without TiO_2 additives after the HF etching.

conversion from TiO_2 to TiC. With the increasing content of TiO_2, the excessive C is also increasingly consumed to form TiC_xO_y. Because of the lack of diffusion barrier for Si, SiO_2 formation is facilitated and its crystallization also accelerates. The general reduction reaction for TiO_2 to TiC is

$$(x+1)\mathrm{TiO_2} + 2\mathrm{C} \rightarrow \mathrm{Ti_xO_y} + \mathrm{TiC} + \mathrm{CO}. \quad (1)$$

Because of the simultaneous presence of TiC, C, Ti_xO_y, SiO_2, and SiOC, we predict that higher pyrolysis temperatures than 1400 °C will lead to the consumption of Ti_xO_y for complete TiC formation as well as the formation of SiC as for conventional SiOC systems, if enough excessive free C is available. Eventually, TiC–SiC–(C) should be obtained.

The microstructure transformation process for the systems without TiO_2 and with TiO_2 can be illustrated in Fig. 2. Without TiO_2, the free carbon content is high and a thick layer of carbon species (outer black layer) separates the SiOC clusters. Because of the isolation of SiOC from other species, the SiOC content (the layer outside of the dashed square) is also relatively high. As a result, the SiO_2 content (within dashed square) is low, as mostly amorphous phase surrounded by excessive C due to limited Si diffusion (Fig. 2a). With the addition of TiO_2, the free carbon phase (outer black layer) is consumed through the formation of TiC. Thus, SiOC is more likely to phase separate and Si can diffuse more freely for SiO_2 cluster formation. SiOC content (the layer outside of the dashed square) is reduced. With the increasing SiO_2 cluster size (within dashed square), it crystallizes into crystalline SiO_2. To verify this growth of the SiO_2 clusters, the samples pyrolyzed at 1400 °C with and without TiO_2 additions have been etched with a HF solution and tested with nitrogen adsorption. Since the TiO_2 size is much larger than the SiO_2 cluster size (25 vs. <10 nm), the SiO_2 cluster size change can be accurately assessed. The resulting pore size distributions (corresponding to the SiO_2 cluster size distribution) for both the samples are shown in Fig. 2c. The SiOC sample without TiO_2 shows a sharp peak at approximately 3 nm and has virtually no pores larger than 8 nm. The sample with TiO_2 has the

same peak at 3 nm but also contains a wider distribution of pores with sizes greater than 10 nm. This experimentally proves the impact of free carbon consumption by the TiC_xO_y formation in increasing the SiO_2 cluster size and the above model.

High temperature oxidation stability

The thermal stability of the SiOC–TiC_xO_y samples during the TGA analysis is shown in Fig. 3a. At 1200 °C pyrolysis temperature, there is a slight weight gain up to 0.25 wt% for all the samples. The TiO_2 content does not play any significant role in the weight gain. At 1300 °C pyrolysis temperature, there is a slight weight gain up to 0.25 wt% for the 0–20 wt% TiO_2 samples; for the 30 wt% TiO_2 sample, a weight loss up to 0.4 wt% is observed. At 1400 °C pyrolysis temperature, the low TiO_2 content samples show the same trend as those at 1200 and 1300 °C pyrolysis conditions. However, there is a substantial weight loss for the 20 and 30 wt% TiO_2 samples starting at ~ 480 °C, up to 12.8 wt% at 1000 °C, showing a continuous deterioration of the higher TiO_2 content samples.

In our previous study, it has been shown that the SiOC matrix is stable in air up to 1000 °C with pyrolysis temperature up to 1400 °C. For the 1400 °C pyrolyzed sample, the stability starts to deteriorate but the total weight loss is still less than 0.5 wt% [31]. Based on the SiOC compositions (free carbon, SiOC, and possibly SiO_2), there are two sources of instability for the SiOC matrix, free carbon, and SiOC clusters.

In the first case, tiny graphene layers with edge carbon atoms can be oxidized; the radical species on the surface of free carbon can also be easily oxidized. The specific oxidation mechanism is the combustion of the carbon free phase:

$$C_{free} + O_2 \rightarrow CO_x. \quad (2)$$

This should lead to weight loss on the TGA curves. Along with Eq. (2), the SiOC units can become more vulnerable to oxidization to SiO_2:

$$SiOC + O_2 \rightarrow SiO_2 + CO_x. \quad (3)$$

SiOC oxidation should lead to weight gain. Combining these two conflicting simultaneous events, and considering that TiC formation is minimal, it explains why only a small weight gain is observed for the samples pyrolyzed at 1200 °C (less free carbon formation to cause weight loss). With the increasing pyrolysis temperature to 1300 °C, some samples have weight loss while others have weight gain. TiO_2 also reacts with the free C in the SiOC matrix during the pyrolysis as shown in Figs. 1 and 2 to form TiC. As a result, weight gain is still observed for the 0–20 wt% TiO_2 samples but substantial weight loss is observed for the 30 wt% TiO_2 samples. With the pyrolysis temperature increase to 1400 °C, all the samples show weight loss; The 0 and 10 wt% TiO_2 samples have weight loss of 0.29 and 1.27 wt%, respectively; the 20 and 30 wt% TiO_2 samples show significant weight loss, up to 12.8 and 10.9 wt%, respectively, at 1000 °C testing temperature. This means that due to

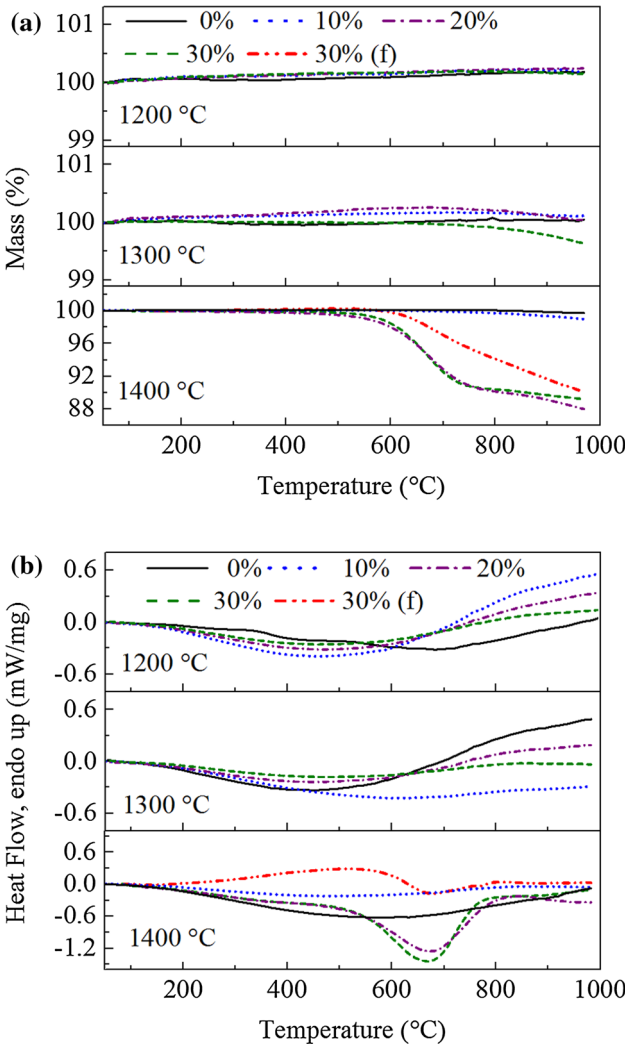

Figure 3 **a** TGA weight change and **b** DSC heat flow curves for the SiOC–TiC_xO_y composites with different TiO_2 contents and at different pyrolysis temperatures.

more extensive phase separation and free carbon formation, the samples with higher pyrolysis temperatures are less stable, especially when the TiO_2 content is high enough to consume the free carbon and 'destabilize' the SiOC system. At the same time, higher pyrolysis temperature leads to a higher tendency for the conversion of TiO_2/Ti_xO_y to TiC; the TiO_2 conversion to TiC is almost complete.

The DSC data for the samples, shown in Fig. 3b, can be used to further understand the oxidation of the samples. For all the samples pyrolyzed at 1200 and 1300 °C, as well as the 0 and 10 wt% TiO_2 samples pyrolyzed at 1400 °C, only a broad exothermic peak is observed. For the 20 and 30 wt% TiO_2 samples pyrolyzed at 1400 °C, a sharp exothermic peak occurs between 550 and 800 °C. This temperature range corresponds to the region at which the majority of mass loss occurs in the TGA data, and the exothermic reaction is indicative of oxidation of the free carbon as previously explained.

To examine the corresponding microstructure changes, the SEM images for the 30 wt% TiO_2 sample after 1200, 1300, and 1400 °C pyrolysis are shown in Fig. 4. At 1200 °C pyrolysis temperature, the microstructure is mostly featureless. The faint roundish features are the original TiO_2 nanoparticles. With the increasing pyrolysis temperature to 1300 °C, a brighter phase starts to appear in localized regions. This is the newly formed phase along with the residual TiO_2 phase. With further pyrolysis temperature increase to 1400 °C, some bright particulate species are clearly visible. We believe that these microstructures show the progression of the TiC phase formation. Since TiC has much higher density (4.93 g/cm^3) than the SiOC matrix species (SiO_2, C, SiOC, 2.2–2.3 g/cm^3; amorphous C, 1.45 g/cm^3) [34], the new phase appearance and presence can be clearly shown.

Based on the drastic weight loss for the high TiO_2 samples and our SEM image observations, it indicates that TiO_2 dispersion in the SiOC matrix has a significant effect on the SiOC matrix stability. To illustrate the effect that surface modification of the original TiO_2 particles has on their dispersion within the SiOC, EDS mappings for Ti, Si, and O with an SEM image for the non-functionalized and functionalized 30 wt% TiO_2 samples pyrolyzed at 1400 °C is shown in Fig. 5. The non-functionalized sample shows several micronsized agglomerates, a broad size distribution of the agglomerates, and

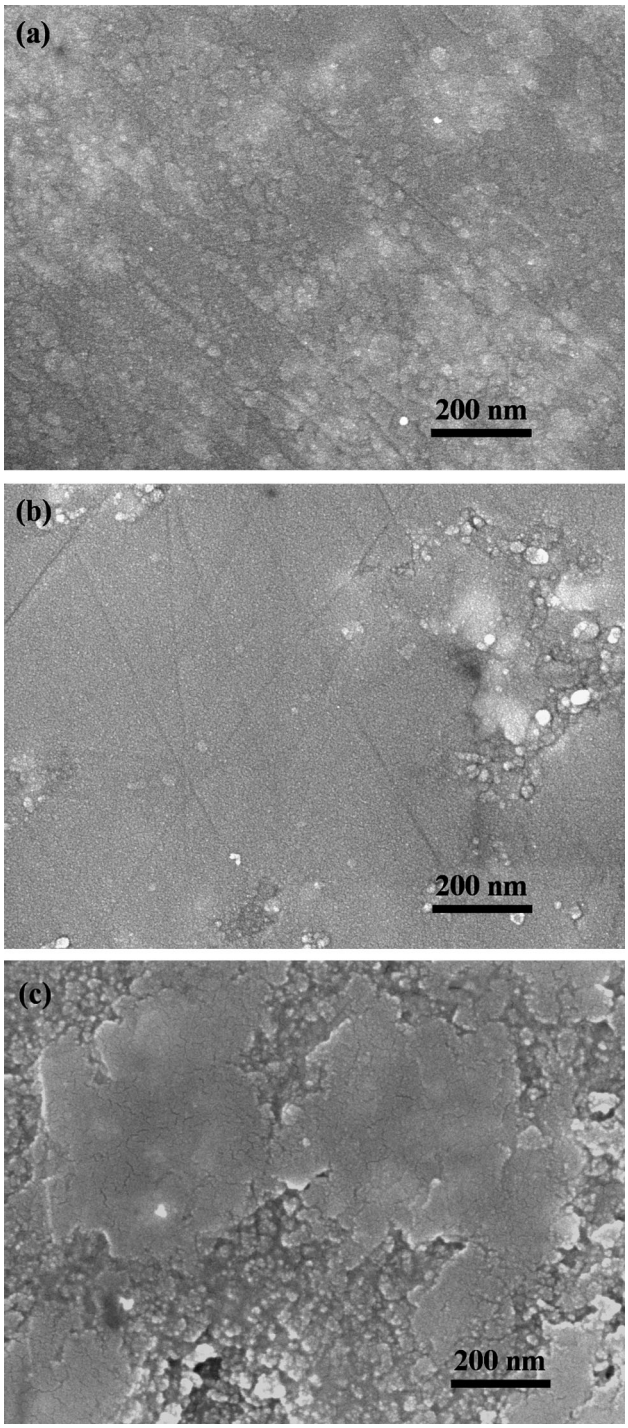

Figure 4 Microstructures of SiOC–TiC samples with 30 wt% TiO_2 content after pyrolysis at **a** 1200 °C, **b** 1300 °C, and **c** 1400 °C.

inhomogeneous distribution of the particles. The functionalized sample also shows agglomerates, but the particles have a more narrow size distribution and better dispersion within the sample. To compare the TiO_2 distribution effect and determine if the

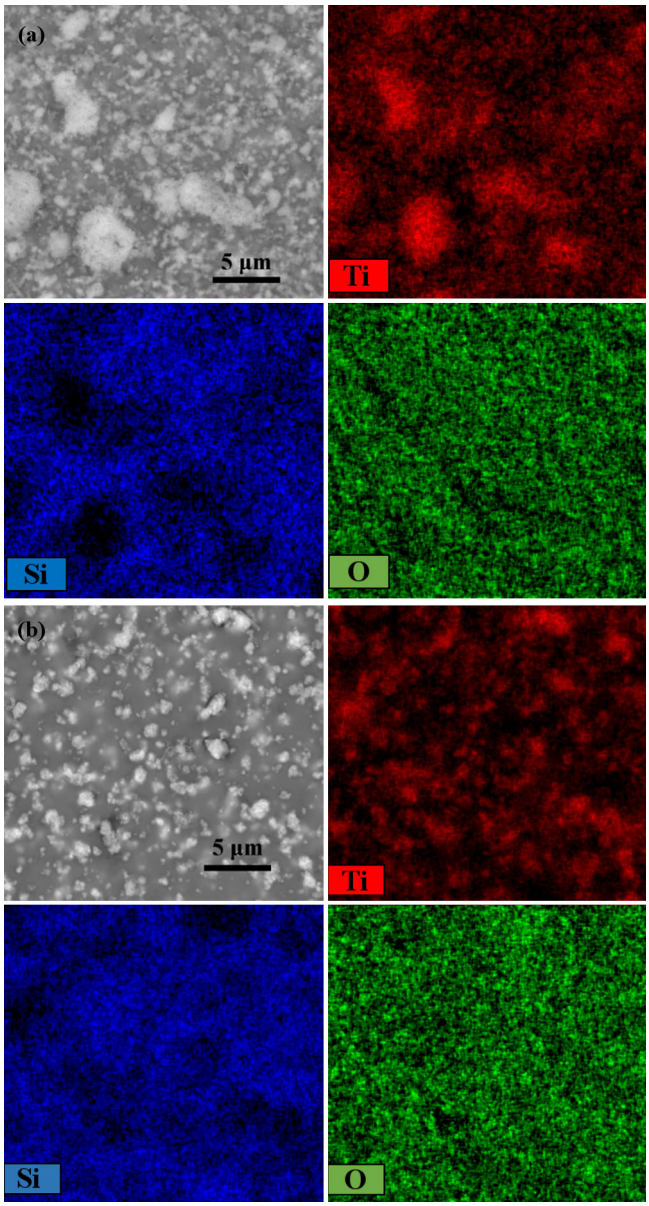

Figure 5 Elemental distribution of Ti, Si, and O for the SiOC–TiC_xO_y samples after the 1000 °C thermal treatment in air: **a** without TiO_2 functionalization and **b** with TiO_2 functionalization.

initial TiO_2 dispersion uniformity in the SiOC matrix can delay the destabilization of the SiOC matrix, the thermal behaviors of the SiOC–TiC_xO_y composite with functionalized TiO_2 after pyrolysis at 1400 °C are also shown in Fig. 3. It shows that with the TiO_2 functionalization, the SiOC–TiC_xO_y system is stable up to approximately 550 °C. With further temperature increase, the final weight loss is 10.5 wt%, slightly lower than the weight loss of the non-functionalized TiO_2 sample, which is at 10.9 wt% as stated earlier. In addition, the DSC data for the functionalized TiO_2 sample do not show a sharp exothermic peak, but rather a much broader exothermic peak; this could explain the slower mass loss rate observed for the functionalized sample.

To fully explore the capacity of this material system for electrical conductivity gain while maintaining thermal stability, further improving the dispersion of the TiO_2 nanoparticles in the SiOC matrix should be pursued. Isolated, individual TiO_2 distribution at high weight percent should enable complete conversion of TiO_2 to TiC, which can significantly increase the electrical conductivity without causing thermal stability loss.

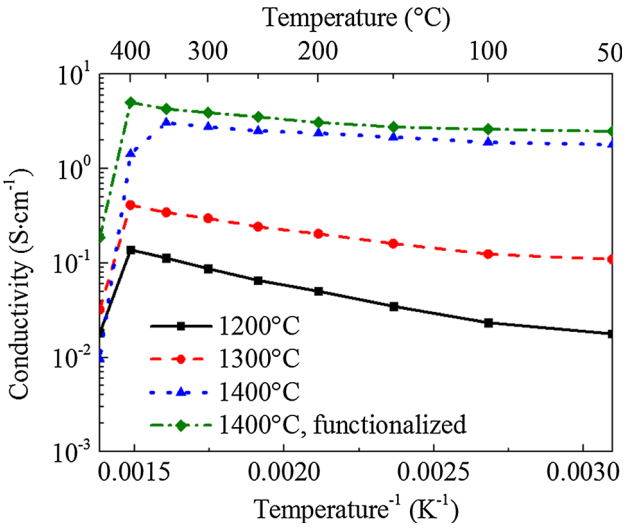

Figure 6 Conductivity change with the pyrolysis temperatures for the SiOC–TiC_xO_y composite at different pyrolysis temperatures.

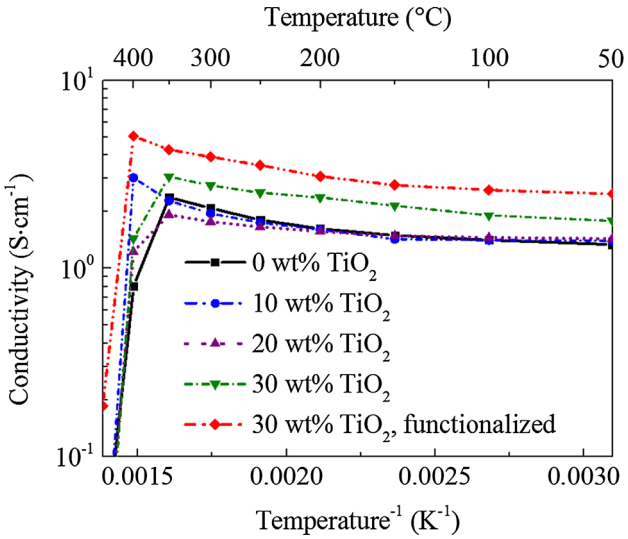

Figure 7 Electrical conductivity for the SiOC–TiC_xO_y composites with 0–30 wt% TiO_2 addition after 1400 °C pyrolysis.

Electrical conductivity

Figure 6 shows the electrical conductivity change with the pyrolysis temperatures for the 30 wt% TiO_2 addition sample. Higher pyrolysis temperatures lead to higher electrical conductivity. At 1200 °C pyrolysis temperature, the conductivity increases from 0.0178 to 0.138 S cm^{-1} from room temperature to 400 °C. At 1300 °C pyrolysis temperature, the conductivity increases from 0.109 to 0.410 S cm^{-1} from room temperature to 400 °C. At 1400 °C pyrolysis temperature, the conductivity ranges from 1.78 S cm^{-1} at room temperature to 3.07 S cm^{-1} at 350 °C. We believe that the increase in the conductivity with the increasing pyrolysis temperatures is a result of increasing TiC formation and free (segregated) carbon content. Based on our earlier work and the literature, for the segregated carbon at high pyrolysis temperatures, a network of graphite-like lamellae of a few atom layers in size can be assumed [35]. With TiO_2 addition and subsequent TiC formation, the conductivity should increase compared to the pure SiOC system of the same composition because of the high electrical conductivity of TiC (5000–7500 S cm^{-1} at room temperature). In addition, TiO_2 to TiC conversion could have led to an increased free carbon content and possibly a structural modification, leading to ordering of the graphitic domains (transformation of sp^3 into sp^2). This is because the possible reactions between TiO_2 and SiOC would lead to SiO_2, TiC, and free carbon following the equation below:

$$TiO_2 + 2SiOC \rightarrow 2SiO_2 + TiC + C. \quad (4)$$

Or, the reactions can split into two reactions:

$$TiO_2 + SiOC \rightarrow SiO_2 + TiOC, \quad (5)$$

$$TiOC + SiOC \rightarrow SiO_2 + TiC + C. \quad (6)$$

Also, the carbon may instead be consumed by the carbothermal reduction of TiO_2 as expressed in Eq. (1), allowing the silica domains to grow due to the loss of carbon. So the two possibilities are phase separation following Eqs. (5) and (6), resulting in SiO_2, TiC, and more free carbon, or the consumption of the carbon layer and subsequent growth of the SiO_2, resulting in SiO_2, TiC, and less free carbon. However, in light of the small amount of TiC formed and the dominant presence of the SiOC matrix, we believe that the free carbon content increases. This in turn can lead to higher electrical conductivity. The exact format of carbon is difficult to quantify due to the small size (as small as 1–2 nm) and intermixing nature in the SiOC matrix. Compared to our earlier reported results for the SiOC derived from PHMS + 60 wt% DVB, this is indeed the case [31]. Without TiO_2 addition, the conductivity ranges from 1.34 S cm^{-1} at room temperature to 2.38 S cm^{-1} at 350 °C. Because of the relatively low volume percent of TiO_2 added, TiC distribution is largely discrete, as

shown in Figs. 4 and 5. Still, it increases the electrical conductivity. In the future, further efforts will be devoted to increase the TiO_2 addition and the resulting TiC content. The electrical conductivity of the expected SiOC–TiC should further improve. It should be noticed that all the samples show a drastic conductivity decrease at ≥400 °C. This is believed to be due to the breakdown of the conductive turbostratic carbon network under the electric field as well as the formation of a surface oxide layer [31]. Even though the SiOC materials are fairly stable at high temperatures, the simultaneous presence of the electric field destroys the conductive path.

The TiO_2 addition into the SiOC and thus TiC formation should increase the electrical conductivity. However, Fig. 5 shows that the TiO_2 dispersion state in the polymer matrix can affect the SiOC–TiC_xO_y stability. This impact also applies to the electrical conductivity, as shown in Fig. 7. Without functionalizing TiO_2 before dispersion in the polysiloxane, there is no difference in conductivity for low TiO_2 addition contents. At 0 wt% TiO_2, the conductivity increase from 1.34 S cm^{-1} at room temperature to 2.38 S cm^{-1} at 350 °C. With 10 and 20 wt% TiO_2 addition, the electrical conductivity shows no obvious difference. With 30 wt% TiO_2 addition, the higher content of TiC formation increases the electrical conductivity from 1.78 S cm^{-1} at room temperature to 3.07 S cm^{-1} at 350 °C. With the functionalization of TiO_2, at 30 wt% TiO_2 content, the conductivity increases to 5.03 S cm^{-1} at 400 °C. With further temperature increase after 400 °C, the conductivity also drastically decreases.

Conclusions

This work focuses on using TiO_2 as an additive to form novel high thermal stability and high electrical conductivity SiOC–TiC_xO_y composites. After pyrolysis of PHMS + DVB derived SiOC at 1200–1400 °C, the volumetric shrinkage is 45–52 %, the ceramic yield is 82–84.5 %, and the resulting SiOC material density is 1.7–2.01 g/cm^3. TiO_2 conversion to TiC increases with the pyrolysis temperature up to 1400 °C by carbothermal reaction with the free carbon. Surprisingly, higher pyrolysis temperature leads to lower thermal stability, mainly due to the destabilization of the SiOC network by the TiC formation and the inhomogeneous distribution of TiO_2. With more homogeneous distribution of TiO_2, the thermal stability of the SiOC–TiC_xO_y composite increases. This family of SiOCs also demonstrates high electrical conductivity. Without TiO_2 functionalization, the highest electrical conductivity is 3.07 S cm^{-1}. With TiO_2 functionalization, the highest electrical conductivity is 5.03 S cm^{-1}. The latter is the highest for air atmosphere condition.

Acknowledgements

We acknowledge the financial support from the Office of Naval Research (N000141410446) and the use of the gas adsorption instrument from the National Center for Earth and Environmental Nanotechnology Infrastructure at Virginia Tech.

Compliance with ethical standards

Conflict of Interest The authors declare that they have no conflict of interest.

References

[1] Greil P (1995) Active-filler-controlled pyrolysis of preceramic polymers. J Am Ceram Soc 78:835–848

[2] Colombo P, Mera G, Riedel R, Soraru GD (2010) Polymer-derived ceramics: 40 years of research and innovation in advanced ceramics. J Am Ceram Soc 93:1805–1837

[3] Greil P (2000) Polymer derived engineering ceramics. Adv Eng Mater 2:339–348

[4] Ionescu E, Linck C, Fasel C, Muller M, Kleebe HJ, Riedel R (2010) Polymer-derived Sioc/Zro_2 ceramic nanocomposites with excellent high-temperature stability. J Am Ceram Soc 93:241–250

[5] Ionescu E, Papendorf B, Kleebe HJ, Poli F, Muller K, Riedel R (2010) Polymer-derived silicon oxycarbide/hafnia ceramic nanocomposites. Part I: phase and microstructure evolution during the ceramization process. J Am Ceram Soc 93:1774–1782

[6] Ionescu E, Papendorf B, Kleebe HJ, Riedel R (2010) Polymer-derived silicon oxycarbide/hafnia ceramic nanocomposites. Part II: Stability Toward decomposition and microstructure evolution at T ≫ 1000 degrees C. J Am Ceram Soc 93:1783–1789

[7] Greil P (1998) near net shape manufacturing of polymer derived ceramics. J Eur Ceram Soc 18:1905–1914

[8] Ma QS, Chen ZH (2007) Electrical resistivity of silicon oxycarbide ceramics fabricated via polysiloxane pyrolysis. Rare Metal Mater Eng 36:619–621

[9] Cordelair J, Greil P (2000) Electrical conductivity measurements as a microprobe for structure transitions in polysiloxane derived si–o–c ceramics. J Eur Ceram Soc 20:1947–1957

[10] Volkmann E, Evangelista LL, Tushtev K, Koch D, Wilhelmi C, Rezwan K (2014) Oxidation-induced microstructural changes of a polymer-derived nextel (tm) 610 ceramic composite and impact on the mechanical performance. J Mater Sci 49:710–719. doi:10.1007/s10853-013-7752-4

[11] Wang KW, Ma BS, Li XQ, Wang YG, An LN (2014) Effect of pyrolysis temperature on the structure and conduction of polymer-derived sic. J Am Ceram Soc 97:2135–2138

[12] Ahn D, Raj R (2011) Cyclic stability and c-rate performance of amorphous silicon and carbon based anodes for electrochemical storage of lithium. J Power Sources 196: 2179–2186

[13] Schulz M (2009) Polymer derived ceramics in MEMS/NEMS—a review on production processes and application. Adv Appl Ceram 108:454–460

[14] Reinold LM, Graczyk-Zajac M, Gao Y, Mera G, Riedel R (2013) Carbon-rich sicn ceramics as high capacity/high stability anode material for lithium-ion batteries. J Power Sour 236:224–229

[15] Graczyk-Zajac M, Toma L, Fasel C, Riedel R (2012) Carbon-rich sioc anodes for lithium-ion batteries: Part I. Influence of material UV-Pre-treatment on high power properties. Solid State Ionics 225:522–526

[16] Hauser R, Francis A, Theismann R, Riedel R (2008) Processing and magnetic properties of metal-containing sicn ceramic micro- and nano-composites. J Mater Sci 43:4042–4049. doi:10.1007/s10853-007-2143-3

[17] Zhou C, Yang L, Geng H et al (2012) Preparation of Si-C-N-Fe magnetic ceramic derived from iron-modified polysilazane. Ceram Int 38:6815–6822

[18] Chen XJ, Su ZM, Zhang L, Tang M, Yu Y, Zhang L, Chen L (2010) Iron nanoparticle-containing silicon carbide fibers prepared by pyrolysis of Fe(Co)(5)-doped polycarbosilane fibers. J Am Ceram Soc 93:89–95

[19] Yurkov GY, Astaf'ev DA, Nikitin LN, Koksharovc YA, Kataevaa NA, Shtykovad EV, Dembod KA, Volkovd AA, Khokhlovb AR, Gubina SP (2006) Fe-containing nanoparticles in siloxane rubber matrices. Inorg Mater 42:496–502

[20] Vakifahmetoglu C, Pippel E, Woltersdorf J, Colombo P (2010) Growth of one-dimensional nanostructures in porous polymer-derived ceramics by catalyst-assisted pyrolysis. Part I: Iron catalyst. J Am Ceram Soc 93:959–968

[21] Vakifahmetoglu C, Colombo P, Carturan SM, Pippel E, Woltersdorf J (2010) Growth of one-dimensional nanostructures in porous polymer-derived ceramics by catalyst-assisted pyrolysis. Part II: Cobalt catalyst. J Am Ceram Soc 93:3709–3719

[22] Guo AR, Roso M, Colombo P, Liu JC, Modesti M (2015) In situ carbon thermal reduction method for the production of electrospun metal/sioc composite fibers. J Mater Sci 50:2735–2746. doi:10.1007/s10853-015-8827-1

[23] Cordelair J, Greil P (2001) Electrical characterization of polymethylsiloxane/$Mosi_2$-derived composite ceramics. J Am Ceram Soc 84:2256–2259

[24] Kim DP (2001) Preparation of electrically conducting sic/$mosi_2$ composites from metal mixtures of preceramic polymer. Mater Res Bull 36:2497–2505

[25] Liu WP, DuPont JN (2003) Fabrication of functionally graded tic/ti composites by laser engineered net shaping. Scr Mater 48:1337–1342

[26] Swift GA, Koc R (1999) Formation studies of tic from carbon coated TiO_2. J Mater Sci 34:3083–3093. doi:10.1023/A:1004692714595

[27] Woo Y-C, Kang H-J, Kim DJ (2007) Formation of TiC particle during carbothermal reduction of TiO_2. J Eur Ceram Soc 27:719–722

[28] Cho D, Park JH, Jeong Y, Joo YL (2015) Synthesis of titanium carbide-carbon nanofibers via carbothermal reduction of titania with carbon. Ceram Int 41:10974–10979

[29] Dewan MAR, Zhang G, Ostrovski O (2008) Carbothermal reduction of titania in different gas atmospheres. Metall Mater Trans B 40:62–69

[30] Gadiou R, Serverin S, Gibot P, Vix-Guterl C (2008) The Synthesis of SiC and TiC protective coatings for carbon fibers by the reactive replica process. J Eur Ceram Soc 28:2265–2274

[31] Lu K, Erb D, Liu M (2016) Thermal stability and electrical conductivity of carbon-enriched silicon oxycarbide. J Mater Chem C 4:1829–1837

[32] Peña-Alonso R, Sorarù GD, Raj R (2006) Preparation of ultrathin-walled carbon-based nanoporous structures by etching pseudo-amorphous silicon oxycarbide ceramics. J Am Ceram Soc 89:2473–2480

[33] Wilson AM, Zank G, Eguchi K, Xing W, Yates B, Dahn JR (1997) Pore creation in silicon oxycarbides by rinsing in dilute hydrofluoric acid. Chem Mater 9:2139–2144

[34] Martinez-Crespiera S, Ionescu E, Kleebe HJ, Riedel R (2011) pressureless synthesis of fully dense and crack-free sioc bulk ceramics via photo-crosslinking and pyrolysis of a polysiloxane. J Eur Ceram Soc 31:913–919

[35] Robertson J (1986) Amorphous-carbon. Adv Phys 35:317–374